arXiv:1406.5027v2 [astro-ph.EP] 15 Jul 2014

Astronomy & Astrophysics manuscript no. 22283˙le
July 16, 2014
© ESO 2014

Low Delta-V near-Earth asteroids: A survey of suitable targets for space missions*

S. Ieva[1,2,3], E. Dotto[1], D. Perna[2], M. A. Barucci[2], F. Bernardi[4], S. Fornasier[2,5], F. De Luise[6], E. Perozzi[7,8,9], A. Rossi[10], J.R. Brucato[11]

[1] INAF - Osservatorio Astronomico di Roma, Via Frascati 33, 00040 Monte Porzio Catone, Rome, Italy
e-mail: simone.ieva@oa-roma.inaf.it
[2] LESIA - Observatoire de Paris, CNRS/UPMC (Paris 6)/Univ. Paris Diderot (Paris 7), 5 place J. Janssen, 92195 Meudon, France
[3] Università di Roma Tor Vergata, Via della Ricerca Scientifica 1, 00133 Rome, Italy
[4] SpaceDyS, Via Mario Giuntini 63, 56023 Cascina, Pisa, Italy
[5] Université Paris Diderot – Sorbonne Paris Cité, 4 rue Elsa Morante, 75205 Paris, France
[6] INAF - Osservatorio Astronomico di Teramo, Via Mentore Maggini snd, 64100 Teramo, Italy
[7] Deimos Space, Ronda de Poniente 19, 28760 Tres Cantos, Madrid, Spain
[8] INAF - IAPS, Via Fosso del Cavaliere 100, 00133 Rome, Italy
[9] ESA - NEOCC, ESRIN, Via Galileo Galilei 64, 00044 Frascati, Rome, Italy
[10] IFAC- CNR, Via Madonna del Piano 10, 50019 Sesto Fiorentino, Firenze, Italy
[11] INAF - Osservatorio Astrofisico di Arcetri, Largo E. Fermi 5, I-50 125 Firenze, Italy

Received: 11 December 2013 / Accepted: 28 June 2014

Abstract

Context. In the past decades near-Earth objects (NEOs) have become very important targets to study, since they can give us clues to the formation, evolution, and composition of the solar system. In addition, they may represent either a threat to humankind or a repository of extraterrestrial resources for suitable space-borne missions. Within this framework, the choice of next-generation mission targets and the characterisation of a potential threat to our planet deserve special attention.
Aims. To date, only a small part of the 11 000 discovered NEOs have been physically characterised. From ground- and space-based observations, one can determine some basic physical properties of these objects using visible and infrared spectroscopy.
Methods. We present data for 13 objects observed with different telescopes around the world (NASA-IRTF, ESO-NTT, TNG) in the 0.4 - 2.5 μm spectral range, within the NEOSURFACE survey. Objects are chosen from among the more accessible for a rendez-vous mission. All of them are characterised by a delta-V (the change in velocity needed for transferring a spacecraft from low-Earth orbit to a rendez-vous with NEOs) lower than 10.5 km/s, well below the solar system escape velocity (12.3 km/s).
Results. We taxonomically classify 9 of these objects for the first time. Eleven objects belong to the S-complex taxonomy, and the other 2 belong to the C-complex. We constrain the surface composition of these objects by comparing their spectra with meteorites from the RELAB database. We also compute olivine and pyroxene mineralogy for asteroids with clear evidence of pyroxene bands. Mineralogy confirms the similarity with the already found H, L, or LL ordinary chondrite analogues.

Key words. Astrobiology – Minor planets, asteroids: NEOs, low delta-V, silicates – Techniques: spectroscopic – Methods: data analysis

1. Introduction

Near-earth objects (NEOs) are the subject of great interest in the scientific community, for both their potential usefulness for future space-borne activities and their importance for the formation and the evolution of the solar system. The current standard model for the solar system's formation predicts that the population of small bodies is the remnant of the process that led to the formation of the planets some 4.6 billion years ago. They are also invoked to explain the actual abundance on inner planets of water and organics. It has also been implied that NEOs could have played an important role in the development of life (Maurette, 2005).

Besides the delivery of water and organics, the investigation of near Earth asteroids (NEAs) and comets is particularly important because they represent a well-known threat to life on our planet. Asteroid impacts, which billions of years ago are supposed to have delivered organics on Earth, pose a significant threat to the whole of human civilization today. Space agencies are nowadays studying mitigation techniques. Most of them, like the kinetic impactor, depend strongly on the composition of the target asteroid.

A high degree of diversity in terms of composition and spectral properties is present amongst the NEA population, with compositions ranging from siliceous to carbonaceous, from basaltic to metallic, necessarily implying completely different internal densities and strengths. The physical properties of more than 85% of the 11 000 NEAs discovered to date are still unknown. The spectroscopy of the asteroid's surface is correlated with the internal composition, hence structure. As such, further spectroscopic observations of NEAs would assist in the charac-

* Based on observations carried out at the European Southern Observatory - NTT (Programs 075.C-0282, 076.C-0577 and 078.C-0141), NASA - IRTF (Program 087) and Telescopio Nazionale Galileo (Sessions AOT14-TAC41, AOT15-TAC69 and AOT26-TAC32.)
Send offprint requests to: S. Ieva

terisation and thus suitability of future space missions. Missions to NEOs have been proven to be both technically feasible and financially viable on a low budget, making them particularly interesting for both national space agencies and private companies (Zimmer & Messerschmid, 2011).

The accessibility from Earth of potential targets of space missions is studied by classical orbital transfer algorithms, like the Hohmann transfer formulation (Prussing, 1992), which gives the minimum energy transfer trajectory between two orbits in space. This algorithm has been used to retrieve delta-V (ΔV), the velocity change needed to be applied to the spacecraft to realise a rendez-vous mission to NEAs (Shoemaker & Helin 1978, Perozzi et al. 2001). NEAs could be an easier target than the Moon or a much more complicated one than Jupiter (Perozzi et al. 2010). In addition, objects with a ΔV lower than the solar system escape velocity (12.3 km/s) are easier to reach for a manned or a robotic exploration.

In this paper we present the result of spectroscopic observations in the visible (0.4 - 0.8 μm) and near infrared ranges (0.9 - 2.4 μm) for 13 NEAs with ΔV lower than 10.5 km/s, as computed by Lance Benner's list[1] of ΔV. These observations were performed in the framework of the NEO-SURFACE survey[2], which is a survey dedicated to the investigation of low ΔV and potentially hazardous asteroids (PHAs).

2. Observations and data reduction

The data presented in this article have been collected with various instruments working in the visible and near-infrared range. They were obtained with the New Technology Telescope (ESO-NTT) at La Silla Observatory (Chile), the NASA Infrared Telescope Facility (NASA-IRTF), located at the Mauna Kea observatory in Hawaii (USA), and the Telescopio Nazionale Galileo (TNG), located at the Roque de los Muchachos Observatory in La Palma, Canary islands (Spain). The observational conditions are reported in Table 1.

2.1. Visible

The visible data presented in this work were obtained during three observational campaigns (June 2005, October 2005 and November 2006) at NTT, and in December 2012 at TNG. At TNG spectra were acquired using the DOLORES detector (Device Optimised for the LOw RESolution), with the low resolution blue (LR-B) grism, spanning the 0.38-0.80 μm range, and a 2 arcsec slit width, oriented along the parallactic angle to reduce the effects of atmospheric differential refraction. At NTT, spectra were acquired using EMMI (ESO Multi Mode Instrument), equipped with the grism #1 and the 5 arcsec slit in RILD (red) mode, to cover the 0.41 - 0.96 μm range.

Data reduction was performed with the software package ESO-Midas using standard procedures, as described in Dotto et al. (2006), Fornasier et al. (2004), and Perna et al. (2010). The basic procedure for converting raw flux measurements to reflectance spectra started with median bias subtraction and flat-field correction. Then, 2-D spectra were collapsed into mono-dimensional spectra, integrating the flux along the spatial axis, with an aperture radius generally between 1.5 and 2 FWHM and subtracting the sky contribution. We performed wavelength calibration identifying different spectral lines from Ne-Ar and He-Ar calibration lamps. We also applied the extinction law for each site and performed extinction correction. The reflectivity was obtained by dividing the spectrum of each asteroid by the one of the solar analogue (usually the one with the closest airmass of the object). Spectra were smoothed with a median-filtering technique where, within a ten-pixel box, the original value was replaced by the median one if the two differed by a set threshold of 10%. Finally spectra were normalised at 0.55 μm.

2.2. Near-infrared

The near-infrared spectra were obtained during three runs at IRTF (August, September, and October 2004), two at TNG (August 2006 and July 2007), and one at NTT in October 2006; we used IRTF equipped with the SpeX instrument (Rayner et al. 2003), a low-resolution prism, with a wavelength range from 0.8 to 2.5 μm and a dispersion of 50 Å per pixel. We used an 0.8 arcsec slit, oriented along the parallactic angle, to reduce atmospheric effects. At TNG we used the Near Infrared Camera Spectrometer (NICS), coupled with the AMICI prism, in low-resolution mode. We covered the 0.9 - 2.4 μm spectral range and used a 2 arcsec slit, always oriented along the parallactic angle. At NTT, spectra were collected using the SofI (Son OF Isaac) instrument in the low-resolution mode, using the blue (0.95 - 1.64 μm) and red grisms (1.53 - 2.52 μm), and then combining the overlapped region.

NIR observations were carried out using the standard technique of moving the objects along the slit between two positions denoted A and B. Cycles are repeated on ABBA sequences until the total exposure time is reached.

Standard procedures were used in the reduction process, as before with the visible data. We corrected spectra for flat field; then, bias and sky removal were obtained by subtracting the two spectra and producing $A-B$ and $B-A$ frames. We combined and averaged all pairs to obtain the final spectrum, which was then extracted. IRTF and NTT spectra were calibrated in wavelength through spectral lines from different calibration lamps (Ne, Ar). For the TNG-NICS, spectral wavelength calibration was obtained using a look-up table available on the TNG website[3]. Extinction and solar removal was carried out by dividing the spectrum of each asteroid by the best solar analogue, generally the one with the closest airmass or the one observed right after or before the asteroid. The NIR spectra of the observed asteroids were normalised at 1.25 μm.

For asteroids (13553) Masaakikoyama, (68359) 2001 OZ13, (203471) 2002 AU4, and (277127) 2005 GW119, we combined our visible data with infrared spectra provided by the MIT-UH-IRTF Joint Campaign for NEO Reconnaissance[4]. The spectra of the asteroids with infrared and visible range were overlapped, merging the common wavelength region using good atmospheric transmission zones to retrieve the normalisation factor, following procedures used by Fornasier et al. (2008).

3. Taxonomic classification and meteorite links

We performed a χ^2 best-fit method between our spectrum and the most representative one of each class of the Bus-DeMeo taxonomy (DeMeo et al. 2009), an extension in the infrared of the SMASSII spectral taxonomy (Bus & Binzel, 2002), spanning a wavelength range between 0.45 to 2.45 μm and finally counting

[1] http://echo.jpl.nasa.gov/~lance/delta_v/delta_v.rendezvous.html
[2] http://www.oa-roma.inaf.it/planet/NEOSurface.html
[3] http://www.tng.iac.es/instruments/nics/spectroscopy.html
[4] http://smass.mit.edu/minus.html

24 classes. The results of our taxonomic classification are reported in Table 2. Eleven asteroids are classified as belonging to the S-complex, while only two NEAs are classified as belonging to the C-complex. Nine of these objects were classified for the first time.

We investigated the suitable meteorite analogue type by comparing the acquired reflectance spectra with laboratory reflectance spectra of meteorites. Such a comparison presents some limitations (Gaffey et al. 2002) associated with the spectral variations due to changes in grain size, viewing geometry, etc. Nonetheless, all of these effects mainly produce a variation in the absorption band contrast, but do not significantly affect the wavelength positions of the absorption features, which are diagnostic for surface composition and therefore give us constraints on it.

Using the M4AST online tool (Popescu et al. 2012), we automatically used a χ^2 method to compare our observed spectra with the whole sample of meteorite spectra included in the RELAB database. For each observed target, we analysed the 50 fits by visual inspection with the lowest χ^2 value given by the tool: to identify the suitable meteorite analogue of each observed NEO amongst them, we checked the presence and position of diagnostic spectral features, we took the meteorite and NEO albedo into account when available, and we considered the overall spectral match with each potential meteorite analogue. By comparing the spectral parameters of our observed bodies with meteorite spectral parameter ranges (see e.g. Clark et al. 2011 and Dunn et al. 2010), we ended up with a few meteorites belonging to the same group, which can be considered as suitable spectral analogues. For each target we suggest a possible meteorite analogue characterised by a low χ^2 value and an overall good-quality fit. Amongst the different meteorites giving similar χ^2 values, we preferred the matches that mimicked diagnostic spectral features over matches that did not. Table 2 reports, for each observed NEO, the meteorite that better reproduces the NEO spectral behaviour, together with its computed χ^2. The matches we suggest are also shown in Figs. 1 - 4.

3.1. The C-complex

In the Bus-DeMeo taxonomy, C-complex classes have weak spectral features. Cg and Cgh-classes for example are characterised by a strong UV drop-off, but the Cg does not have a 0.7 μm feature, which also appears in the Ch (See Bus (1999) and DeMeo et al. (2009)). In our survey only two asteroids seem to belong to the C group: (13553) Masaakikoyama has a classification of a Cg-type, while (203471) 2002 AU4 seems to belong to C/Cg-type (Fig. 1).

Krugly et al. (2006) found for **(13553) Masaakikoyama** a rotation period of 38 hours. Reddy et al. (2006) observed this asteroid in the near infrared and found an excess of thermal emission and estimated an albedo of 0.03 ± 0.01, in agreement with a carbonaceous composition. They also suggest an association with CV carbonaceous types. The visible spectrum we acquired, combined with the NIR spectrum taken from the MIT-UH-IRTF Joint Campaign, is flat without any features and with a possible UV drop-off below 0.5 μm, suggesting a Cg-type classification. On the basis of the analysis of spectral parameters and the overall spectral behaviour, we found agreement with CK and CM carbonaceous chondrite meteorites; also taking the low albedo of the asteroid into account, which is more compatible with a CM classification, we suggest the CM2 Y86695 as meteorite analogue.

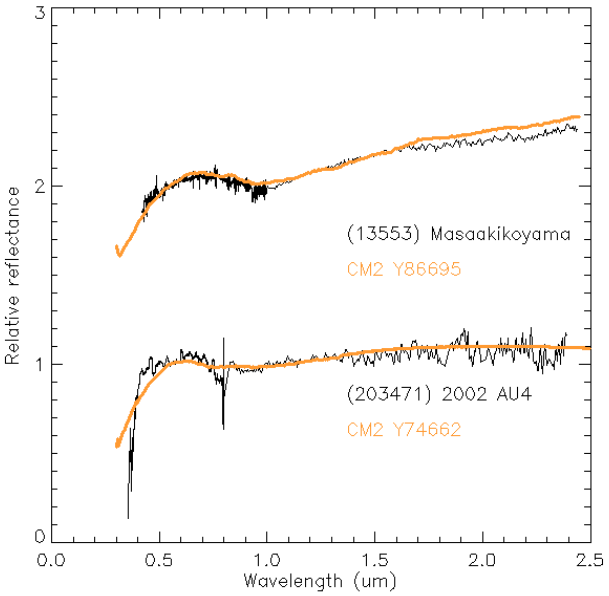

Figure 1. Visible spectra of C-complex asteroids (13553) Masaakikoyama and (203471) 2002 AU4 with their meteorite analogues, combined with the NIR spectra made available by the MIT-UH-IRTF Joint campaign for NEO Reconnaissance. The spectra are normalised at 0.55 μm and shifted for clarity.

The visible spectrum we obtained for **(203471) 2002 AU4** is flat and slightly bluish, with a possible feature around 0.75 μm. We classified 2002 AU4 as a C or a possible Cg-type. We also found a good match with the spectra of CM carbonaceous chondrite meteorites. In Fig. 1 we report the observed spectrum and the one of the CM2 meteorite Y74662.

3.2. The S-complex: S, Sa, Sv, Sr-types

Objects that reside in the S-complex are identified by the 1 and 2 μm features with shallow absorption bands. There is also a subtle classification (Sa, Sr, Sq, Sv) according to the exact depth and position of spectral bands. When spectra are extended in the near-infrared, many S-objects became less and less separated. In our survey two asteroids belong to the Sv class, (85804) 1998 WQ5 and (145656) 4788 P-L; one object exhibits a Sr spectrum: (138883) 2000 YL29; one remains in the original S-class: 2004 TD10 (Fig. 2)

Oey (2006) found a rotation period of P = (3.0089 ± 0.0001) h for asteroid **(85804) 1998 WQ5**, and Mainzer et al. (2011) estimated an albedo of 0.24. Its spectrum shows a minimum around 0.9 μm and a shallow band at 2 μm. We classified it as an Sv-type and found general agreement with the spectral parameters of H ordinary chondrite meteorites. The spectrum of the ordinary chondrite H4 Chela is able to reproduce the general spectral behaviour and to match the band around 0.9 μm.

Thomas et al. (2011) find an albedo of 0.19 for **(138883) 2000 YL29** and suggest an Sq-type classification. The NIR spectrum we observed is very red in the 0.9-1.4 μm region, with the presence of a possible absorption band at 0.9 μm and another around 2.0 μm. We suggest a possible Sr-classification. Our observed spectrum exhibits general agreement with L ordinary chondrite meteorites. In Fig. 2 we show it with the one of the ordinary chondrite L6 Bruderheim, which gives the lowest χ^2 value and is able to reproduce the general spectral behaviour.

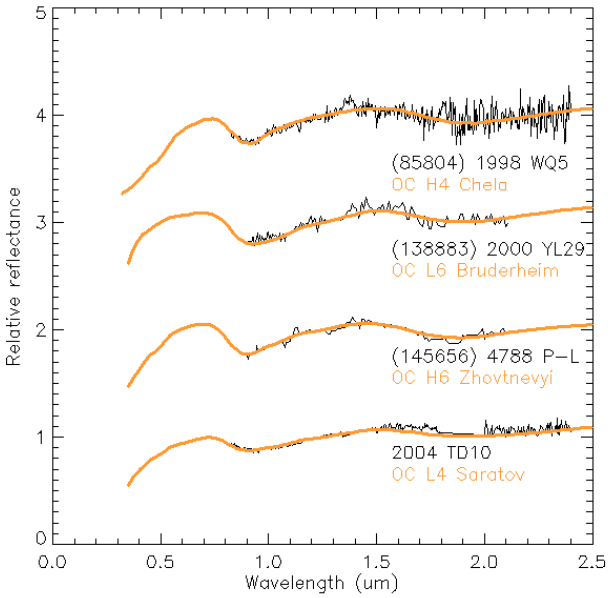

Figure 2. NIR spectra of S-complex asteroids (85804) 1998 WQ5, (138883) 2000 YL29, (145656) 4788P-L, and 2004 TD10 with their meteorite analogues. The spectra are normalised at 1.25 μm and shifted for clarity.

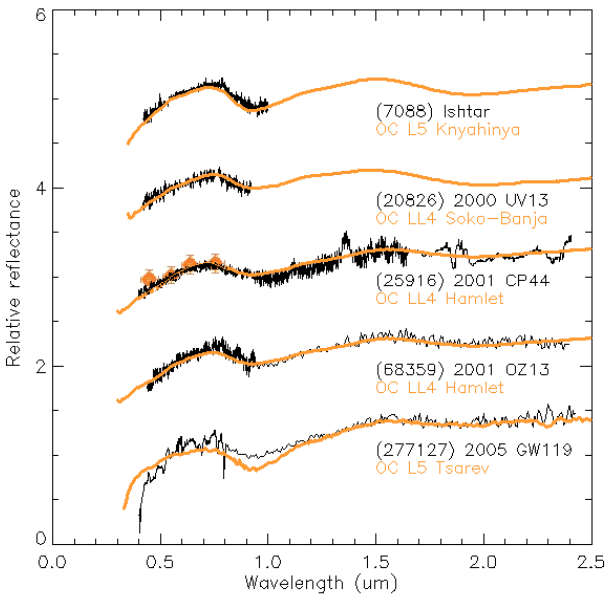

Figure 3. Visible-NIR spectra of S-complex asteroids (7088) Ishtar, (20826) 2000 UV13, (25916) 2001 CP44, (68359) 2010OZ13, and (277127) 2005GW119 with their meteorite analogues. For (68359) 2010OZ13 and (277127) 2005GW119, we combined our visible spectra with the NIR data available in the MIT-UH-IRTF public database. The spectra are normalised at 0.55 μm and shifted for clarity.

The NIR spectrum we acquired for **(145656) 4788 P-L** is somewhat red, and it shows a possible absorption band at 1.0 μm and another around 1.9 μm. We classified it as an Sv-type. On the basis of comparison of our spectrum with laboratory spectra of meteorites in the RELAB database, we suggest a possible link with H ordinary chondrite meteorites; in particular, we show the comparison with the H6 Zhovtnevyi in Fig. 2. Their spectral parameters match the general spectral behaviour of this NEA.

We observed **2004 TD10** two weeks after the discovery. The spectrum has a high S/N, but the regions around 1.4 μm and around 1.9 μm were removed due to the high residuals of atmospheric bands. The S-type nature of this asteroid is suggested by the two absorption bands: a clear one at 1 μm, and a shallower one at 2 μm. We found general spectral agreement with L ordinary chondrite meteorites like the L4 Saratov shown in Fig. 2, which has spectral behaviour that is very similar to this NEA.

3.3. The S-complex: Sq/Q types

In the near-infrared, Q and Sq types are very similar to each other, with a broadened and rounded 1 μm band that reaches a minimum reflectance level around 0.9-0.95 μm and a band around 2 μm, similar to olivine and pyroxene assemblages. Q-types show a moderately steep UV slope shortwards of 0.7 μm, Sq-types can contain a relatively strong feature around 0.63 μm, and some of them exhibit also another feature around 1.3 μm. In our survey seven objects are classified as Sq types: (25916) 2001 CP44, (68359) 2001 OZ13, (164222) 2004 RN9, (277127) 2005 GW119, (7088) Ishtar, (20826) 2000 UV13, and (142464) 2002 TC9 (Figs. 3 and 4). For the last three, a classification as Sr type cannot be excluded.

The object **(7088) Ishtar** is a binary asteroid with a slope parameter G = 0.24 (Pravec et al. 2012). Reddy et al. (2007) used lightcurve analysis to obtain an estimate of the synodic orbital period of (20.63±0.02) h. They also made the assumption that the primary has an a spheroidal shape, giving its rotation period of P = (2.6786±0.0002) h and a lightcurve amplitude of 0.11 mag. The visible spectrum we obtained is very red until 0.75 μm and shows a prominent band around 0.95 μm, suggesting an Sq or Sr-type classification. However, owing to the binary nature of this asteroid, rotationally resolved spectra obtained in different geometrical view are needed to distinguish between possibly different compositions of the pair. We found general agreement between our observed spectrum and those of ordinary chondrite meteorites belonging to the L class. In Fig. 3 we show the comparison with laboratory spectrum of the L5 ordinary chondrite Knyahinya, which gives the lowest χ^2 value and matches the overall spectral behaviour.

The asteroid **(20826) 2000 UV13** was observed by Binzel et al. (2004), who classified it as belonging to the Sq class. It has an estimated albedo of 0.18 (Thomas et al. 2011) and a rotation period of 12 hours[5]. The visible spectrum we obtained is red until 0.75 μm and shows a possible 0.9 μm band, but infrared data are needed to confirm it. It could be either classified as an Sq or Sr-type. The reflectance spectrum agrees with those of LL meteorites: we found a match with the LL4 Soko-Banja, whose spectrum is shown in Fig. 3.

Based on images taken during three different nights, Elenin & Molotov (2012) find a rotation period for **(25916) 2001 CP44** of P= (4.19± 0.01) h and a light curve amplitude of 0.28 mag. Thomas et al. (2011) classified this object as a Q-type with an albedo of 0.21. In the visible range we observed this object with EMMI, using both the imaging and spectroscopic modes. Our photometric data allowed us to obtain the colours B - V = (0.819±0.020), V - R = (0.463±0.013), and V - I = (0.789±0.013). The spectrum shows a moderately red slope. The NIR spectrum we obtained has two absorption features at 1 and

[5] http://www.asu.cas.cz/~ppravec/newres.txt

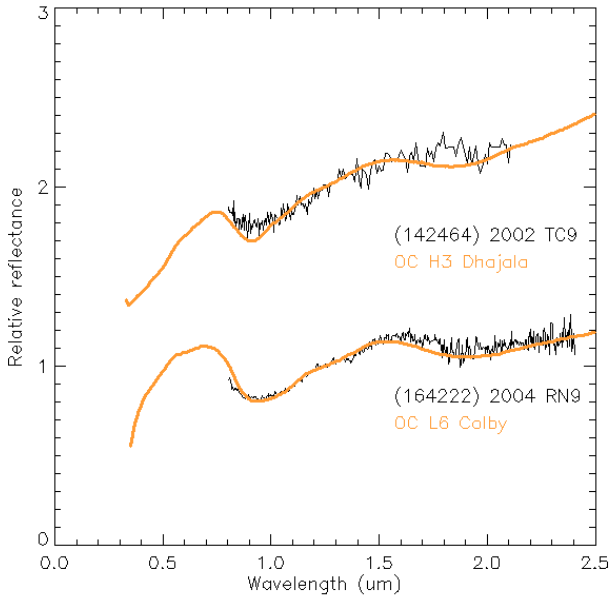

Figure 4. NIR spectra of S-complex asteroids (142464) 2002 TC9 and (164222) 2004 RN9 with their meteorite analogues. The spectra are normalized at 1.25 μm and shifted for clarity.

2 μm, which are typical of the silicate asteroids, in particular of an Sq-type. Meteorites that reproduce the observed spectral behaviour better are those belonging to the LL group of ordinary chondrites. In particular, we report the spectrum of LL4 ordinary chondrite Hamlet in Fig. 3.

Within the ExploreNEO survey, Thomas et al. (2011) estimated an unusual albedo of $0.47^{+0.32}_{-0.22}$ and an Sq spectral type for **(68359) 2001 OZ13**. We acquired two visible spectra forty minutes away from each other. No sign of rotational variation has been found: both spectra appear very red until 0.78 μm, and afterwards there is the 0.9 μm absorption band. Our spectrum, combined with the NIR data available in the MIT-UH-IRTF Joint Campaign, confirm its classification as an Sq-type. The best meteorite analogues we found belong to the LL class. In particular, we show the match we obtained with the ordinary chondrite LL4 Hamlet in Fig. 3.

Combining the visible spectrum we observed for **(277127) 2005 GW119** with the infrared spectrum available in the ,literature (MIT-UH-IRTF Joint Campaign) we classified it as an Sq-type. Ordinary chondrites belonging to the L class match the observed spectrum, but there is some discrepancy in the 1 μm region, where the meteorite spectra generally lead to underestimating the observed one. In Fig. 3 we report the spectrum, along with the one of the ordinary chondrite L5 Tsarev, which is able to better reproduce the diagnostic spectral feature at 1 μm.

Mainzer et al. (2011) find an albedo of 0.12 for **(142464) 2002 TC9**. The NIR spectrum we obtained suggests this asteroid is an Sq or Sr-type, with an absorption band at 1 μm but a reddish slope behaviour around 2 μm. We found general agreement with H ordinary chondrite meteorites, and in Fig. 4 we report our comparison with the H3 Dhajala, whose spectrum matches the wavelength position of the diagnostic 1 μm band better.

The object **(164222) 2004 RN9** has a NIR spectrum that shows absorption bands around 0.9 μm and 1.9 μm, in agreement with an Sq-type classification. L-ordinary chondrites generally agree with the overall spectral behaviour of the asteroid; in particular, we chose the spectrum of the L6 Colby, which matches the wavelength position of the 1 and 2 μm band (Fig. 4) better.

4. Mineralogy analysis

As mentioned before, S-type asteroids exhibit a generally red spectrum with prominent bands in the NIR region, typically of pyroxene and olivine assemblages, around 1 and 2 μm. These absorption bands are caused by the presence of Fe^{2+} cations located in the M2 crystallographic site (Adams, 1974, 1975; Burns, 1993).

There are multiple parameters that are usually compared in the literature to infer the mineralogy properties of silicate asteroids, such as band minimum, band centres (BI and BII), band depth, band width, and band area ratio (BAR, between the 2 and the 1 μm bands) (Gaffey et al. 2002). The ones that are used the most are band minimum and centre, the lowest point of the reflectance spectrum, before and after continuum removal, respectively. The continuum in this case is defined as the linear slope between the relative maxima, generally located around 0.7 and 1.4 μm.

To compute band minimum we fitted a six-degree polynomial over the bottom third of each band. Errors were computed using a Monte Carlo simulation, randomly sampling data 100 times and taking the standard deviation as incertitude. Theoretically, to determine the band centre, we should subtract the continuum properly from the asteroid's spectrum. But to apply this technique, we should have the visible and NIR spectra taken at the same time, since different observation conditions could result in markedly different spectral slopes, hence the subsequent band centre determination. For this reason, we preferred to compute band minima and use laboratory determinations to derive band centres. We used the simple relation between band minimum and band centre described by Cloutis & Gaffey (1991)

$$BI = BI_{min} + 0.007\,\mu m \pm 0.004. \quad (1)$$

Since the start position for Band I and the end position for Band II are not always available in our spectra, to compute the band areas we fitted a six-degree polynomial over each band by considering the starting point around 0.7 μm for Band I and for Band II the furthest point around 2.5 μm. We computed the band area first by dividing out the continuum and then measuring the area between the new continuum and the polynomial fit for the 1 and 2 μm bands. BAR was subsequently obtained by dividing Band II area by Band I area.

BAR measurements are also affected by temperature shifts, so to compare our measurements with laboratory data, we used an inverse correlation found by Sanchez et al. (2012) for different assemblages of olivine and orthopyroxene, e.g. BAR correction decreases when the temperature increases. We established an approximate surface temperature using a standard thermal model (Lebofsky & Spencer, 1989):

$$T = [(1 - A)L_{\odot}/16\,\epsilon\eta\sigma\pi r^2]^{1/4}. \quad (2)$$

where A stands for the bond albedo of the asteroid, $L_{\odot}$ is the solar luminosity, σ the Boltzman constant, and r the distance from the Sun in metres. For our computations we assumed that the beaming factor η is approximately 1 and the infrared emissivity $\epsilon \sim 0.9$. The final temperature however is not particularly sensitive to minor changes in these parameters or to changes in the albedo. For objects with unknown albedo we considered the mean one of their taxonomical classes (0.15 for an S-type, 0.04

for a C-type), as taken from Shestopalov & Golubeva (2011). Once we found an approximate temperature for the surface of the asteroids, we applied Sanchez's relation to retrieve BAR correction:

$$BAR_{corr} = 0.00075 \times T(K) - 0.23. \quad (3)$$

We inferred mineralogy properties by applying formulas derived by Dunn et al. (2010) and used also by Dunn et al. (2013) to study the relationships between fayalite (Fa) in mafic minerals and ferrosilite (Fs) in pyroxene and spectral features. These equations were obtained for ordinary chondrites and theoretically could be applied to asteroids that share a similar mineralogy. With these relationships it is possible to determine the molar content of fayalite in olivine, ferrosilite in pyroxene, and also the relative percentage of olivine and pyroxene. The correlation between BI and the molar content of Fa and Fs can be expressed as a second-order polynomial fit:

$$Fa = -1284.9 \times (BI)^2 + 2656.5 \times (BI) - 1342.3, \quad (4)$$

$$Fs = -879.1 \times (BI)^2 + 1824.9 \times (BI) - 921.7, \quad (5)$$

while the mineral ratio between olivine and pyroxene can be calculated from BAR values, using the relationship

$$ol/(ol + px) = -0.242 \times BAR + 0.728. \quad (6)$$

We were able to calculate BI and the BAR values for four objects (2004 TD10, (25916) 2001 CP44, (85804) 1998 WQ5, and (164222) 2004 RN9). For (68359) 2001 OZ13, (142464) 2002 TC9, and (277127) 2005 GW119 we computed BI, though it was not possible to determine the BAR owing to the low S/N in the Band II region. The derived olivine and pyroxene chemistries are shown in Figs. 5-7. Figure 5 shows BAR vs BI for our targets, along with the Gaffey classification for olivine-orthopyroxene assemblages, where the S(IV) subgroup represents the mafic silicate components of ordinary chondrites. In Fig. 6 we plot the molar content of Fs vs Fa, as found with the Dunn et al. (2010) relations. In Fig. 7 the same values are plotted against the olivine and pyroxene ratio, along with compositional regions for H, L, and LL found by Dunn et al. (2010). Band centres, BARs and slopes are shown in Table 3.

In Fig. 5 (25916) 2001 CP44 is just above the polygonal region defined by Gaffey et al. (1993) for the ordinary chondrites, near the LL-chondrite region, and just above the mixing line of olivine-ortopyroxene, as described in Cloutis & Gaffey (1986). Its values of Fa and Fs are consistent with those derived by LL ordinary chondrites by Dunn et al. (2010), which give a range for fayalite between (26 – 32) ± 1.3 mol% and between (22 – 26) ± 1.4 mol% for ferrosilite. The relative olivine percentage estimated from BAR for this asteroid also agree with spectrally-derived measurements reported by Dunn et al. (2010) for LL ordinary chondrites (Fig. 7), which give ol/(ol+px) values in the (0.58 – 0.69) ± 0.03 range, and a specific value for the Hamlet chondrite of 0.59. We conclude that this asteroid could be consistent with an LL ordinary chondrite, in agreement with the best meteoritic analogue we found by spectral comparison.

The asteroid (85804) 1998 WQ5 in Fig. 5 and in Fig. 7 falls just outside the H-chondrite region. Nevertheless, its pyroxene chemistry is located in the range estimated for H chondrites (Fig. 6), in agreement with the meteorite analogue we found, the ordinary chondrite H4 Chela. Despite some inconsistencies among Figs. 5, 6, and 7, this asteroid could be coherent with an H chondrite.

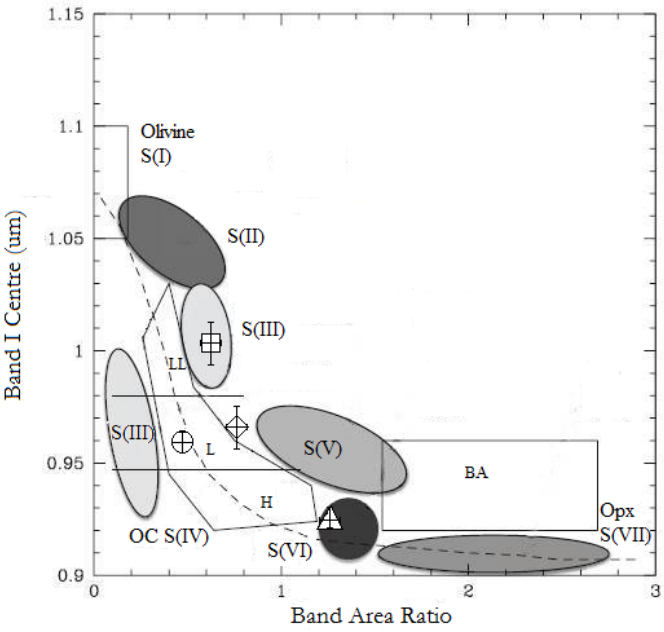

Figure 5. Plot of BI versus BAR for (25916) 2001 CP44 (square), (85804) 1998 WQ5 (triangle), (164222) 2004 RN9 (circle), and 2004 TD10 (diamond). The rectangular zone includes pyroxene-dominated basaltic achondrite (BA) assemblages. The S(IV) subgroup represents mafic silicate components of ordinary chondrites (OC), from Gaffey et al. (1993). The dashed curve is the limit of the mixing line for olivine and orthopyroxene mixing, as shown in Cloutis & Gaffey (1986). Horizontal lines separate H, L, and LL chondrites. Adapted from Gaffey et al. (1993).

The BI and the BAR of (164222) 2004 RN9 place it in the region corresponding to L ordinary chondrites (Fig. 5). This is in strong agreement with the meteoritic analogue we found, the L6 ordinary chondrite Colby. Using the equations for molar contents, we determined olivine and pyroxene chemistries consistent with those derived by Dunn et al. (2010) for L ordinary chondrites (i.e. Fa between (21 – 27) ± 1.3 mol% and Fs between (17 – 23) ± 1.4 mol%). From the BAR value we estimated the composition of olivine and pyroxene, in agreement with spectrally-derived measurements reported by Dunn et al. (2010) for L ordinary chondrites, having a relative percentage of olivine between (0.54 – 0.62) ± 0.03 (Fig. 7).

In Fig. 5 2004 TD10 is just outside the bounds of the S(IV) region, in the L chondrites zone, in agreement with the meteoritic analogue that we found, the chondrite L4 Saratov. According to our calculations, the olivine and pyroxene chemistries are consistent for values for L chondrites derived by Dunn et al. (2010). The ol/(ol+px) ratio found for this asteroid also agrees with the Dunn et al. (2010) measurements for L ordinary chondrites.

5. Conclusions

We collected seven spectra in the visible and seven in the near infrared range from different telescopes (NASA-IRTF, ESO-NTT, TNG) for 13 NEAs with a low ΔV. These targets are all suitable candidates for future space missions.

Through the analysis of the spectra obtained, we estimated surface composition of these asteroids, yielding classifications

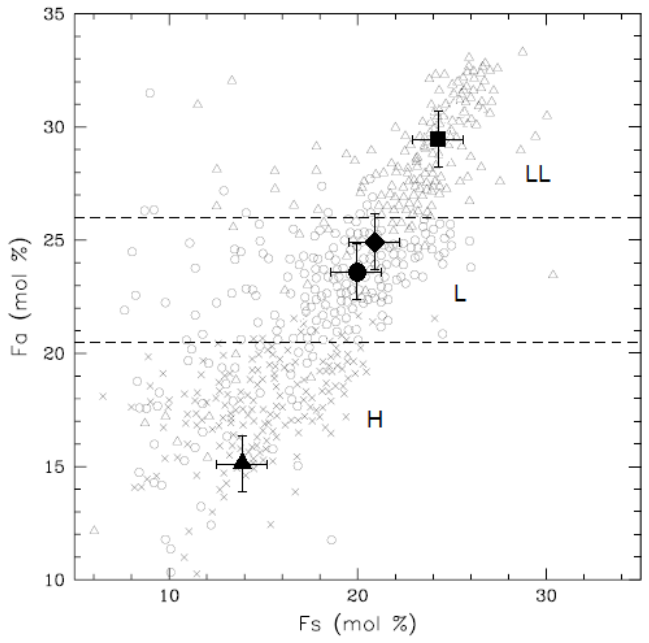

Figure 6. Molar content of Fa vs. Fs for NEAs (25916) 2001 CP44 (square), (85804) 1998 WQ5 (triangle), (164222) 2004 RN9 (circle), and 2004 TD10 (diamond), along with values for LL (open triangles), L (open circles), and H (x) ordinary chondrites, adapted from Sanchez et al. (2013). The error bars correspond to the values determined by Dunn et al. (2010) 1.4 mol% for Fs and 1.3 mol% for Fa. The horizontal dashed lines represent the approximate boundaries for H, L, and LL chondrites.

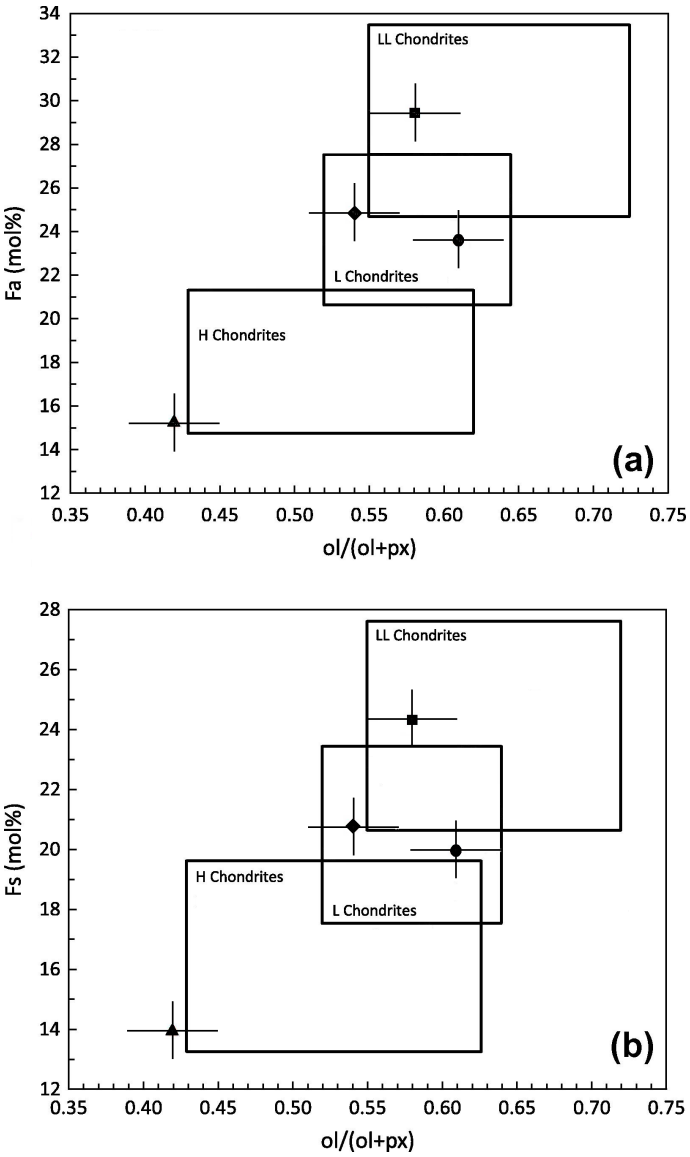

Figure 7. (a) Spectrally derived mol% Fa and (b) mol% Fs plotted as a function of derived ol/(ol+px) for (25916) 2001 CP44 (square), (85804) 1998 WQ5 (triangle), (164222) 2004 RN9 (circle), and 2004 TD10 (diamond). Solid boxes represent the range of spectrally derived ol/(ol+px) for H, L, and LL ordinary chondrites, together with error bars from Dunn et al. (2010). Error bars represent the least mean square of the errors (0.03 for ol/(ol+px), 1.3 mol% for Fa, and 1.4 mol% for Fs). Adapted from Dunn et al. (2013).

according to Bus & DeMeo taxonomy. We found 11 S-complex objects and two C-complex objects. In particular, four objects are Sq-types, three Sq/Sr-types, two Sv-types, and two exhibit a S or Sr spectrum, while there are two C/Cg-types. Through the comparison of the observed NEAs and the RELAB meteorite database, we obtained good matches between ordinary chondrites and S-type asteroids and between carbonaceous chondrites and C-type asteroids. Finally, we investigated mineralogy by sampling the prominent bands in the NIR, which is typical of olivine and pyroxene assemblages. We obtained good agreement with the previous meteorite analogues we found and with the overall results from Dunn et al. (2010).

Visible and NIR spectroscopic observations are fundamental for defining the physical characteristics of the NEO population and resolving the conundrum about the prevailing abundance among NEOs. The high rate of silicate asteroids, which until only recently were seen to be the dominant component of the NEO population, could be in principle a selection effect, as suggested by the NEOWISE survey (Masiero et al. 2011), or is more probably due to the high efficiency of the transport mechanisms in the inner main belt, where Q and S-type asteroids are most commonly found (Fieber-Beyer et al. 2012).

The physical characterisation of an asteroid is generally the first step towards developing and designing any space mission to a target asteroid, such as a mitigation mission or a rendez-vous mission. Spectral characterisation of NEOs is a powerful tool for defining successful mitigation strategies in the case of possible impactors, since there is a high degree of diversity among the composition of NEO population. For a kinetic impactor mitigation mission, the stress waves produced by an impact propagate and attenuate differently in a C-type or in an S-type, since the whole process strongly depends on the asteroid's porosity.

Missions to NEOs are becoming more and more feasible, and ground-based spectroscopic surveys, like NEO-SURFACE, are a fundamental step in the broader framework of the NASA's FY2014 Asteroid Strategy, which as stated by President Obama in 2010, has the aim of sending a human mission to an asteroid by 2025. The selection of a future target would be strongly affected by the low ΔV and the peculiarities of its spectrum. We therefore need to observe and classify the largest possible number of these low ΔV-asteroids.

Acknowledgements. We would like to thank all the telescope operators for their contribution. In this article we make use of meteorite spectra taken with the

NASA RELAB facility at Brown University. Part of the data utilised in this publication were obtained and made available by the MIT-UH-IRTF Joint Campaign for NEO Reconnaissance. The IRTF is operated by the University of Hawaii under Cooperative Agreement no. NCC 5-538 with the National Aeronautics and Space Administration, Office of Space Science, Planetary Astronomy Program. The MIT component of this work is supported by NASA grant 09-NEOO009-0001 and by the National Science Foundation under Grants Nos. 0506716 and 0907766. Part of this work was supported by INAF (PRIN-INAF 2009 Near Earth Objects) and ASI (A.A. ASI I/079/9/0) funds. We would like also to thank the anonymous referee, for the thoughtful suggestions and comments, which helped us improve the manuscript.

References

Adams, J. B. 1974, JGR, 79, 4829
Adams, J. B. 1975, in Infrared and Raman spectroscopy of lunar and terrestrial minerals. Academic Press, San Diego, 91.
Binzel, R. P., Rivkin, A. S., Stuart, J. S. et al. 2004, Icarus, 170, 259
Burns, R. G. 1993, in Mineralogical applications of crystal field theory, Cambridge univ. press, Cambridge
Bus, S.J. 1999, PhD Thesis, MIT
Bus, S.J. & Binzel R. P. 2002, Icarus, 158, 146
Clark, B. E., Binzel, R. P., Howell, E. S. et al. 2011, Icarus, 216, 462
Cloutis, E. A. & Gaffey, M. J., Jackowski, T. L., Reed, K. L. 1986, JGR, 91, 11641
Cloutis, E. A. & Gaffey, M. J. 1991, JGR, 96, 22809
DeMeo, F. E., Binzel, R. P., Slivan, S. M., Bus, S. J. 2009, Icarus, 202, 160
Dotto, E., Fornasier, S., Barucci, M. A. et al. 2006, Icarus 183, 420
Dunn, T. L., McCoy, T. J., Sunshine, J. M., McSween, H. Y. 2010, Icarus 208, 789
Dunn, T. L., Burbine, T. H., Bottke, W. F., Clark, J. P. 2013, Icarus 222, 273
Elenin, L. & Molotov I. 2012, MPBu, 39, 101
Fieber-Beyer, S. K., Gaffey, M. J., Hardersen, P. S., Reddy, V. 2012, Icarus, 221, 593
Fornasier, S., Dotto, E., Barucci, M. A., Barbieri C. 2004, A&A, 421, 353
Fornasier, S., Migliorini A., Dotto E., Barucci, M. A. 2008, Icarus, 196, 119
Fowler, J. W. & CHillemi, J.R. 1992, in The IRAS Minor Planetary Survey, Philips Laboratory Hanscom Air Force Base, Massachussets.
Gaffey, M. J., Burbine, T. H., Piatek, J. L. et al. 1993, Icarus, 106,573
Gaffey, M. J., Cloutis, E. A., Kelley, M. S., Reed, K. L 2002 in Asteroids III, ed. W. F. Bottke Jr., A. Cellino, P. Paolicchi, and R. P. Binzel, University of Arizona Press, Tucson, 183
Krugly, Yu. N., Gaftonyuk, N. M., Belskaya, I. N. et al. 2007, IAUS, 236, 385
Lebofsky, L. A., & Spencer, J. R. 1989, in Asteroids II, University of Arizona Press, Tucson, 128
Mainzer, A., Grav, T., Bauer, J. et al. 2011, ApJ 743, 156
Masiero, J. R., Mainzer, A. K., Grav, T. et al. 2011, ApJ 741, 68
Maurette, M. 2005, in Micrometeorites and the mysteries of our origin. Springer-Verlag, Berlin/Heidelberg
Oey, J. 2006, MPBu, 33, 96
Perna, D., Dotto, E., Lazzarin, M. et al. 2010, A&A, 513, L4
Perozzi, E., Rossi, A., Valsecchi, G. B. 2001, P&SS, 49, 3
Perozzi, E., Binzel, R. P., Rossi, A., Valsecchi, G. B. 2010, European Planetary Science Congress 2010, 750
Popescu, M., Birlan, M., Nedelcu, D. A. 2012, A&A, 544, 130
Pravec, P., Harris, A.W., KuÅnirk, P., Gald, A., Hornoch, K. 2012, Icarus, 221, 365
Prussing, J.E., 1992, JGCD, 15, 1037
Rayner, J. T., Toomey, D. W., Onaka, P. M. et al. 2003, PASP, 115, 362
Reddy, V., Gaffey, M. J., Abell, P. A., Hardersen, P. S. 2006, 37th Lunar and Planetary Science Conference, LPI, 37, 1746
Reddy, V., Dyvig, R., Pravec, P. et al. 2007, 38th Lunar and Planetary Science Conference, LPI, 38, 1239
Sanchez, J. A., Reddy, V., Nathues, A. et al. 2012, Icarus, 220, 36
Sanchez, J. A., Michelsen, R., Reddy, V., Nathues, A. 2013, Icarus 225, 131
Shestopalov, D. I. & Golubeva, L. F., 2011, 42nd Lunar and Planetary Science Conference, LPI,42, 1608, 1028
Shoemaker, E. M. & Helin, E. F., 1978, NASCP, 2053, 245
Thomas, C. A., Trilling, D. E., Emery, J. P. et al. 2011, AJ, 142, 85
Zimmer, A. K. & Messerschmid, E. 2011, AA 69, 11, 1096

Table 1. Observational circumstances.

Object	ΔV (km/s)	Date	Δ (AU)	r (AU)	Telescope/ Instrument	Spectral range	T_{exp} (s)	Airmass	Solar Analogue (airmass)
(7088) Ishtar	6.684	31/10/05	0.518	1.289	NTT - EMMI	V	400	1.6	SA 93-101 (1.7)
(13353) Masaakikoyama	6.678	19/06/05	0.297	1.274	NTT - EMMI	V	300	1.2	SA 107-684 (1.1)
(20826) 2000 UV13	10.452	20/06/05	1.942	2.411	NTT - EMMI	V	600	1.0	HD 218251 (1.1)
(25916) 2001 CP44	8.219	26/10/06	1.296	2.227	NTT - SofI	NIR	16 x 120	1.0	SA 115-271 (1.0)
		15/11/06	1.400	2.344	NTT - EMMI	V	360	1.1	HD 2141 (1.2)
(68359) 2001 OZ13	6.539	31/10/05	0.582	1.512	NTT - EMMI	V	300	1.1	HD 2141 (1.1)
		31/10/05			NTT - EMMI	V	600	1.2	SA 98-978 (1.1)
(85804) 1998 WQ5	9.541	23/08/04	1.094	1.997	IRTF - SpeX	NIR	14 x 120	1.1	SA 112-1333 (1.1)
(138883) 2000 YL29	7.633	15/07/07	0.700	1.069	TNG - NICS	NIR	28 x 120	1.4	HD 148642 (1.8)
(142464) 2002 TC9	6.934	19/08/06	0.352	1.269	TNG - NICS	NIR	12 x 120	1.0	SA 115-271 (1.0)
(145656) 4788 P-L	7.401	15/07/07	0.312	1.156	TNG - NICS	NIR	8 x 120	1.2	HD 144873 (1.1)
(164222) 2004 RN9	6.436	23/09/04	0.113	1.114	IRTF - SpeX	NIR	16 x 120	1.1	HD 1368 (1.1)
(203471) 2002 AU4	10.025	20/12/12	0.103	1.065	TNG - DOLORES	V	780	1.2	SA 115-271 (1.1)
(277127) 2005 GW119	6.063	20/12/12	0.325	1.290	TNG - DOLORES	V	1800	1.2	SA 115-271 (1.1)
2004 TD10	10.127	21/10/04	0.049	1.028	IRTF - SpeX	NIR	50 x 120	1.6	HD 218251 (1.6)

NOTE: Δ and r are the topocentric and the heliocentric distance, respectively.

Table 2. Physical characteristics of the targets: absolute magnitude, albedo, diameter, taxonomical class, suitable meteorite analogue class, best match analogue, and χ^2 value.

Object	H	ρ_V	D[1] (km)	Tax. class	Meteorite class	Meteorite name	χ^2
(7088) Ishtar	17.08	...	...	**Sq/Sr**	OC L	L5 Knyahinya	3.20×10^{-4}
(13353) Masaakikoyama	16.71	0.03	3.49	**Cg**	CC CM	CM2 Y86695	1.14×10^{-3}
(20826) 2000 UV13	13.70	0.18	5.70	Sq/Sr	OC LL	LL4 Soko-Banja	2.60×10^{-4}
(25916) 2001 CP44	13.40	0.21	6.06	Sq	OC LL	LL4 Hamlet	1.14×10^{-3}
(68359) 2001 OZ13	17.80	0.47	0.53	Sq	OC LL	LL4 Hamlet	7.20×10^{-4}
(85804) 1998 WQ5	15.30	0.24	2.36	**Sv**	OC H	H4 Chela	5.90×10^{-4}
(138883) 2000 YL29	16.70	0.19	1.39	Sr	OC L	L6 Bruderheim	7.80×10^{-4}
(142464) 2002 TC9	18.10	0.12	0.92	**Sq/Sr**	OC H	H3 Dhajala	3.03×10^{-3}
(145656) 4788 P-L	16.35	...	...	**Sv**	OC H	H6 Zhovtnevyi	1.19×10^{-3}
(164222) 2004 RN9	20.66	...	...	**Sq**	OC L	L6 Colby	6.20×10^{-4}
(203471) 2002 AU4	19.20	...	...	**C/Cg**	CC CM	CM2 Y74662	3.14×10^{-3}
(277127) 2005 GW119	18.49	...	...	**Sq**	OC L	L5 Tsarev	8.10×10^{-3}
2004 TD10	22.03	...	...	**S**	OC L	L4 Saratov	3.10×10^{-4}

NOTE: References. (1) Fowler & Chillemi, 1992.
In bold asteroids taxonomically classified for the first time.

Table 3. Visibile slopes, band centres, BARs, and mineralogical composition.

Object	Slope[a] (%/10^3 A)	BI (μm)	BAR	BAR corr	Fa (mol%)	Fs (mol%)	Ol / ol + opx
(7088) Ishtar	12.24 ± 0.03	0.952 ± 0.003	...	...	...	...	...
(13353) Masaakikoyama	4.27 ± 0.17	...	...	...	...	...	...
(20826) 2000 UV13	10.37 ± 0.31	...	...	...	...	...	...
(25916) 2001 CP44	10.00 ± 0.23	1.003 ± 0.009	0.72 ± 0.05	0.62 ± 0.05	29.5 ± 1.3	24.3 ± 1.4	0.58 ± 0.03
(68359) 2001 OZ13	16.13 ± 0.35	0.992 ± 0.005	...	...	...	...	...
(85804) 1998 WQ5	...	0.924 ± 0.005	1.35 ± 0.05	1.27 ± 0.05	15.3 ± 1.3	13.9 ± 1.4	0.42 ± 0.03
(138883) 2000 YL29	...	...	...	...	...	...	...
(142464) 2002 TC9	...	0.925 ± 0.004	...	...	...	...	...
(145656) 4788 P-L	...	...	...	...	...	...	...
(164222) 2004 RN9	...	0.959 ± 0.005	0.52 ± 0.05	0.48 ± 0.05	23.6 ± 1.3	19.9 ± 1.4	0.61 ± 0.03
(203471) 2002 AU4	0.07 ± 0.16	...	...	...	...	...	...
(277127) 2005 GW119	13.23 ± 0.97	0.937 ± 0.003	...	...	...	...	...
2004 TD10	...	0.966 ± 0.010	0.79 ± 0.05	0.76 ± 0.05	24.9 ± 1.3	20.8 ± 1.4	0.54 ± 0.03

NOTE: [a] Computed between 0.5-0.75 μm.